Chemical Engineering Journal 352 (2018) 459–468

Contents lists available at ScienceDirect

Chemical Engineering Journal

journal homepage: www.elsevier.com/locate/cej

High-throughput fabrication of porous carbon by chemical foaming strategy for high performance supercapacitor

Tian Ouyang[a,1], Tianyu Zhang[a,1], Huizhong Wang[b], Fan Yang[c], Jun Yan[a], Kai Zhu[a], Ke Ye[a], Guiling Wang[a], Limin Zhou[b], Kui Cheng[a,b,*], Dianxue Cao[a,*]

[a] Key Laboratory of Superlight Material and Surface Technology of Ministry of Education, College of Material Science and Chemical Engineering, Harbin Engineering University, Harbin, China
[b] Department of Mechanical Engineering, The Hong Kong Polytechnic University, Hung Hom, Kowloon, Hong Kong Special Administrative Region
[c] College of Science, Northeast Agricultural University, Harbin 150030, China

HIGHLIGHTS

- A gas foaming strategy is adopted to prepare the 3D hierarchical porous carbon.
- $NaHCO_3$ is used as activator based on its multistep pyrolysis process.
- The HPC shows high specific capacitance and outstanding stability.

ARTICLE INFO

Keywords:
Hierarchical porous carbon
Chemical foaming
$NaHCO_3$ activation
Supercapacitor

ABSTRACT

Inspired by people to make flour food, a one-pot, low-cost, green and environmental friendly gas foaming strategy is adopted here to prepare the three-dimensional hierarchical porous carbon (HPC) by introducing $NaHCO_3$ as foaming and activation agent. During the pyrolysis process, the CO_2 gas produced during the transforms from $NaHCO_3$ into Na_2CO_3 will resulted in the producers of the macro-pores and meso-pores, meanwhile, the as-produced Na_2CO_3 further reactor with the carbon intermediate at a high temperature, and finally result in forming a micro-pores porous structure. Such intimate structural interconnectivities provide three-dimensional continuous pathway for electron rapid transfer and the interconnected pores allow for the ion to penetrate and evenly contact the electrode material quickly. The electrochemical performance of HPC exhibits a high specific capacitance of 350 F g^{-1} at 1 A g^{-1} and outstanding electrochemical stability with capacitance retention up to 97% after 10,000 cycles. Moreover, the as-assembled symmetric supercapacitor exhibits an ultrahigh energy density of 27.4 Wh kg^{-1}, much higher than most of carbon-based supercapacitors. These results demonstrate a straightforward environment friendly method to mass-produce economical, robust carbon materials as promising candidates for supercapacitor application.

1. Introduction

The global challenges with the rapidly increasing of environmental pollution and energy consumption faced by society today have stimulated tremendous interest in not only exploiting renewable energy sources but also developing high-performance energy storage devices [1,2]. Different with batteries store the energy through *Faradic* reactions, electrical double layer capacitors (EDLCs) based on carbon materials accumulate charges at the interface between electrode and electrolyte, thus endows them the characteristics of high power density, high efficiency and superior cycle life time [3,4]. Therefore, EDLCs are considered as one of the promising electrochemical energy storage devices to bridge the gap between batteries and electrolytic capacitor [5,6]. However, the relatively low energy density compared with battery has largely hindered their application prospects, and has actuated considerable interest in exploring carbon materials for further increasing the specific capacitance without sacrificing their power density [7,8].

In general, the energy density of EDLCs is mainly determined by the specific surface area (SSA) which is the basic factor for ion electro-

* Corresponding authors.
E-mail addresses: chengkui@hrbeu.edu.cn (K. Cheng), caodianxue@hrbeu.edu.cn (D. Cao).
[1] These authors contributed equally to this work.

https://doi.org/10.1016/j.cej.2018.06.184
Received 18 April 2018; Received in revised form 16 June 2018; Accepted 29 June 2018
Available online 30 June 2018
1385-8947/

adsorption to form an electrical double layer and the micro-pores existing in carbon materials are benefited for increasing the SSA [9]. Whereas, the power density is strongly depended on the charge and discharge rate, and the narrow and tortuous channels of micro-pores are disadvantageous for rapid ion and electron transfer [10,11]. Thus, designing a carbon material with fully utilized high SSA and hierarchical three-dimensional cellular network with interconnected pore structure is proposed to fulfil these aims of high energy and power densities [11]. Various synthetic methods such as template mediated synthesis [12–15], physical and chemical activation with assist of water vapor, CO_2 and/or Na/KOH etc. [5,16–18], have been explored for the synthesis of HPC. The templating strategy normally exhibits a powerful pore size control, high SSA, and other size-/surface-dependent properties. However, the removal of templates is a fussy process which will introduce the toxic chemicals [19]. HPC obtained from physical and chemical activation methods usually demonstrated a high SSA and specific capacitance. Nevertheless, the employ multi-step purification procedures slow down this technology for scale-up.

In addition, looking for environmental friendly and renewable natural resources instead of common fossil fuel precursors (for instance, petroleum coke [20], pitch [21] and coal [22]) is another essential and highly desirable concerns for future practical application of carbon nanomaterials in the EDLCs. Very recently, HPC materials derived from biomasses (such as tofu [23], willow catkin [24], flour [25], bacterial cellulose [26], etc.) have received increasing attention from the scientific community due to it is available in high quality and huge amount, and is an environmentally friendly renewable resource [23,27–30]. Besides, the unique organic texture of biomass could also serve as a biotemplate for the formation of a porous structure. More important, using biomass as carbon precursors could incorporate foreign elements into carbon, which has been proven to be an efficient and effective way to tune the intrinsic chemical and electrical properties of carbon, eg. enhancing the electrical conductivity and the wettability, maximizing the electro-active surface area and increasing the capacitance of carbon materials by inducing pseudocapacitive behavior [31–33]. Unfortunately, the previous reports of porous carbon derived from biomass are mostly first carbonization of carbon precursor and follow with a physical and/or chemical activation process. Therefore, developing an environmentally friendly and inexpensive approach to fabricate HPC materials is still a great scientific and engineering challenge.

In this work, inspired by the flour food making process, we have proposed a chemical foaming strategy to form a tunable honeycomb-like HPC by using flour as carbon precursor and baking soda ($NaHCO_3$) acts as an activation agent. The as-prepared HPC realized a high specific capacitance of 350 F g^{-1} at 1 A g^{-1} in 6 mol L^{-1} KOH and outstanding electrochemical stability with capacitance retention up to 97% after 10,000 cycles which is benefit from the large SSA (1376 m^2 g^{-1}), excellent interconnectivity porous structure. In addition, the as-assembled symmetric supercapacitor exhibits an ultrahigh energy density of 27.4 Wh kg^{-1}, much higher than most of carbon-based supercapacitors. We demonstrated potential applications of such one-pot, low-cost, green and template-free method to high-throughput fabrication of HPC as electrodes for high performance supercapacitors application.

2. Experiment

2.1. Synthesis of HPC

HPC was prepared through a facile one-step pyrolysis of the mixture of flour precursor and $NaHCO_3$. In a typical process, 6 g flour with different mass $NaHCO_3$ was first mixed with 75 mL water to obtain a paste, and then dried at 80 °C for 24 h. The resulting product was put into a laboratory tube furnace under argon gas conditions to carbonize. Heating rate was set as 5 °C min^{-1} and the holding time was set as 120 min. Then, the product was washed with 1 mol L^{-1} HCl solution and distilled water, and dried at 80 °C for 12 h in a vacuum oven. The samples described are designated as HPC-T-*x* (T: synthesis temperature, *x*: the mass amount of $NaHCO_3$). For instance, HPC-1000-3 stands for the N-doped porous carbon synthesized at 1000 °C with 3 g $NaHCO_3$.

For comparison, carbon material was prepared by mixture of flour precursor (6 g) and Na_2CO_3 (1.89 g) and denoted as PC-1000.

3. Materials characterization

The surface morphology of as-prepared samples were characterized by field-emission scanning electron microscopy (FESEM, Hitachi SU-8000F), whereas transmission electron microscopy (TEM) images were acquired on a JEM-2010FEF TEM operating. Fourier transform infrared (FT-IR) spectroscopy was carried out with a spectrum 100 from PerkinElmer. X-ray powder diffraction was conducted using a Rigaku TTR III diffractometer with Cu Kα radiation. Raman spectra was obtained by using a Renishaw inVia Raman microscope with an excitation wavelength of 532 nm. The elemental analysis was performed with an elemental analyser (Vario Micro cube). The surface elemental composition was determined by X-ray photoelectron spectroscopy with Al Kα radiation (XPS, Thermo ESCALAB 250). Thermogravimetric analysis was conducted on a TGA/DSC 1600HT (TGA, Mettler Toledo) analyzer and the sample was heated from room temperature to 1000 °C at a heating rate of 10 °C min^{-1} with N_2 flow rate of 50 mL min^{-1}. N_2 adsorption/desorption measurements were characterized by N_2 adsorption at 77 K on a Tristar II 3020 (Micrometritics, USA). All samples were degassed at 150 °C under vacuum for 10 h before the measurements. The specific surface area was calculated by the modified Brunauer-Emmet-Teller (BET) method and the pore size distribution of the samples was obtained by the DFT method.

4. Electrochemical measurements

To fabricate an electrode for the electrochemical measurements, the as-obtained HPC materials were first mixed with carbon black and PTFE in a mass ratio of 90:5:5 to form slurry and then coated onto the nickel foam with coating area of 1 cm^2 and last dried at 100 °C for 12 h in a vacuum oven. Finally, the as-prepared Ni foam was pressed 60 s under 10 MPa pressure to obtain an electrode with thickness of 0.337 mm. The mass loading of each electrode is around 3 mg cm^{-2} which is measured by a microbalance (d = 0.01 mg). Electrochemical performances were measured in a three-electrode system and a two-electrode system, respectively. In the three-electrode system, the cyclic voltammetrys (CVs), galvanostatic charging-discharging (GCD) tests and electrochemical impedance spectroscopy (EIS) were performed using a computerized potentiostat (Autolab PGSTAT302, Eco Chemie) controlled by GPES software in 6 mol L^{-1} KOH aqueous solution. For a two-electrode system, two electrodes with the same size and mass loading were assembled with a glassy fibrous separator, and the electrochemical measurements were measured in 1 mol L^{-1} Na_2SO_4 aqueous solution. All solutions were made with analytical grade chemical reagents and Milli-Q water (18 MΩ cm). Electrochemical impedance spectroscopy (EIS) measurements were carried out by applying an AC voltage with 5 mV amplitude in a frequency range from 0.01 Hz to 100 kHz at the open circuit potential. The specific capacitance of the electrodes can be calculated from the discharge curves according to the following equation:

$$C_g = \frac{I \times \Delta t}{m \times \Delta V} \quad (1\text{-}1)$$

where C_g (F g^{-1}) is specific capacitance based on the mass of the active materials, I (A) is the constant charge/discharge current, Δt (s) is the discharge time, ΔV (V) is the discharge voltage excluding the IR drop, m (g) is the mass of the active materials of electrode.

The energy density (E) and power density (P) were calculated as the following equation:

$$E = \frac{1}{2}CV^2 \quad (1\text{-}2)$$

$$P = \frac{E}{\Delta t} \quad (1\text{-}3)$$

where C ($F\,g^{-1}$) represents the specific capacitance of the supercapacitor measured from the Eq. (1-1), V (V) refers to the discharge potential range that is exclusive of the IR drop, Δt (s) is the discharge time, E ($Wh\,kg^{-1}$) is the energy density, and P ($W\,kg^{-1}$) is the power density.

5. Results and discussion

Wheat flour is a kind of common food raw materials which comes from wheat that is the second largest crop in terms of planting area and yield around the entire world. The composition of flour (ESI Table S1) mainly consisting of carbohydrate (73.5%) and protein (11%), which make it to be considered as a suitable carbon precursor to prepare hierarchical activated carbon materials [28]. However, the general chemical activation process to explore the specific surface area is using KOH, which is highly corrosive for the industrial equipment. In order to answer this issue, in this paper, inspired by the flour food making process, that is adding baking soda ($NaHCO_3$) into the flour pasta to obtain food production with the feature of soft and porous (such as steamed bread, baozi and steamed sponge cake etc.), we have proposed a novel chemical foaming strategy for high-throughput fabrication of HPC materials, as illustrated in Fig. 1a. The SEM image (Fig. S1a) and TEM image (Fig. S1b) reveal that the wheat directly calcined at 1000 °C exhibits a dense and block particle morphology. By contrast, the carbonization of $NaHCO_3$-introduced wheat flour lead to form a 3D scaffolding framework assembled by gauze-like nanoflakes (Fig. 1b and c), analogous to the Chinese flour food (insert of Fig. 1b) and the thickness of carbon wall is ~60 nm (Fig. 1d). The fine structure of the HPC-1000-3 sample was further investigated by TEM, evidently confirms the existing of meso-pores (blue circle marked in Fig. 1e) and micro-pores (red circle marked in Fig. 1f). Such distinct 3D interconnected porous characteristics could efficiently shorten ion diffusion pathway and enhance the electron transfer rate, and further boost the capacitance performance. In addition, partially graphitized area was also found on the HRTEM image, shown by the blue arrow, which will serve as the "highway" for the electron transfer and thus benefit for the rate performance enhancement[34,35]. The XRD patterns (Fig. 1g) exhibit two broader at 2θ of ~24° and ~44°, analogous to the (0 0 2) and (1 0 0) planes of graphite, and the peak intensity of HPC-1000-3 is weaker than that of HPC-1000-0, indicating a decreased degree of graphitization and crystallinity due to the existence in more pores and defects. The same conclusion can also be drawn from the Raman spectra (Fig. 1h), in which a high I_D/I_G ratio of HPC-1000-3 (0.987) compares with HPC-1000-0 (0.954) means the existence of highly disordered carbon. Furthermore, the XPS as shown in Fig. S2 indicates the chemical identities of the heteroatoms in the HPC-1000-3 sample. The N1s XPS is of bad quality with 0.86%, which is too low to be considered doping. The O content of HPC-1000-3 is calculated to be 5.66 at.%, which can not only contribute pseudocapacitance to the overall capacitance and also enhance the wettability of the electrode [36].

To better understand the activation mechanism of $NaHCO_3$, the carbonization process of the mixture (the mass weight of flour and $NaHCO_3$ are 6 g and 3 g, respectively) was first characterized by TG under Ar atmosphere, and the result is performed in Fig. 2a. In the first stage, a 20.7% weight loss below 200 °C is observed, which can be attributed to the evaporation of the water physically adsorbed on the surface, trapped in the intercrystallite pores, and intercalated in the interlayer space[37]. The derivative thermogravimetric (DTG) curve shows a peak located at 242 °C with a ~17.1 wt% weight loss, which is corresponding to the decomposition of $NaHCO_3$ into Na_2CO_3 (Eq. (1-4)). One interesting phenomenon during this stage is the volume of mixture expands significantly as a result of the CO_2 gas escape (the inset of Fig. 2a). The followed ~10.1% weight loss at the temperature range of 200–600 °C is might ascribed to the carbonization of the wheat flour. The last two peaks of DTG curves at 852 and 950 °C with the last 25.3% weight loss can be resulted from the further fusion of Na_2CO_3 (the fusion point of Na_2CO_3 is about 851 °C) and as well as the chemical reaction between carbon with the decomposition product of Na_2CO_3. The as-prepared produces before washing with HCl solution were subjected to XRD (Fig. S3) analysis to characterize the composite materials structure. The existence of Na_2CO_3 (PDF#37-0451) in as-prepared samples of HPC-800-3 and Na_2O (PDF#65-2978) in HPC-900-3 indicate that $NaHCO_3$ decomposed into Na_2CO_3 and part of the Na_2CO_3 decomposed into Na_2O at 900 °C. On the contrary, the XRD pattern of HPC-1000-3 shows two broad peaks corresponding to carbon with no obvious peaks of Na_2CO_3 and other compounds, meaning a uniform activation reaction between C and Na_2CO_3 at 1000 °C. Therefore, the followed reactions may occur based on the above observations.

$$2NaHCO_3 \rightarrow Na_2CO_3 + CO_2 + H_2O \quad (1\text{-}4)$$

$$Na_2CO_3 \rightarrow Na_2O + CO_2 \quad (1\text{-}5)$$

$$Na_2CO_3 + 2C \rightarrow 2Na + 3CO \quad (1\text{-}6)$$

$$Na_2O + C \rightarrow 2Na + CO \quad (1\text{-}7)$$

$$C + CO_2 \rightarrow 2CO \quad (1\text{-}8)$$

Thus, the formation of hierarchical porosity is mainly attributed to the above reactions between carbon and intermediate products. During these processes, the oxygen-rich atmosphere may cause oxidative etching out of carbon atoms and to be replaced by oxygen atoms.

The N_2 adsorption-desorption isotherms were performed to further distinguish the porosity differences between the $NaHCO_3$ activator and carbon intermediate at different temperature, and the results are summarized in Table 1. As presented, the HPC-600-3 sample displays a type I isotherm (Fig. 2b) with little micropores and mesopores (Fig. 2c and Table S2†) and exhibits a macroporous structure (Fig. 2d and g), indicating the CO_2 gas foaming by $NaHCO_3$ decomposition (reaction (1-1)) produces the macropores. To verify this conjecture, the sample of PC-1000, which was prepared by using Na_2CO_3 as activator for comparison, exhibited a relative high SSA (about 739 $m^2\,g^{-1}$) with a V_{micro} of 0.248 $cm^3\,g^{-1}$ and a V_{meso} of 0.156 $cm^3\,g^{-1}$ but not obvious macroporosity structure (Fig. S4). With the temperature increased, the product samples reveal a type IV shape isotherm that have a strong adsorption quantity rising at a low-pressure area (about 0.05) corresponding to N_2 filling in the channel of micro-pores, and a H4-type hysteresis loop at P/P_0 about 0.5 ~ 0.9 indicating the existence of meso-pores. The pore size distribution (PSD) (Fig. 2c) shows that the samples obtained at the calcined temperature beyond 600 °C possess a co-existing feature of micropores and mesopores, and interestingly, different with that of HPC-800-3 and HPC-900-3, the pore distribution of HPC-1000-3 display bimodal and show small populations of pores with dimensions centered at 115 nm, corresponding to small numbers of macroporous structures, which is consistent with the results of TEM (Fig. S5). Besides, the pore wall becomes thinner with the temperature increased (Fig. 2d, e and f), which indicated the completely activation reaction between C and as-produced Na_2CO_3. As a result, the HPC-1000-3 sample exhibited the highest surface area of 1376 $m^2\,g^{-1}$, the biggest total pore volume of 0.992 $cm^3\,g^{-1}$ consist of V_{micro} (0.357 $cm^3\,g^{-1}$) and V_{meso} (0.635 $cm^3\,g^{-1}$). Based on our observations, the formation mechanism of as-prepared HPC mainly content two stages as illustrated in Fig. 2g. In the first stage, the CO_2 gas produced during the transforms from $NaHCO_3$ into Na_2CO_3 will result in the producers of the macro-pores and meso-pores. As followed, the obtained Na_2CO_3 further reactor with the as-formed carbon precursor at a high temperature (Eqs. (1-5)–(1-8)). In other words, the micro-pores existing in the as-prepared carbon materials was came from the activation of Na_2CO_3, and the meso-pores and macro-pores are generated

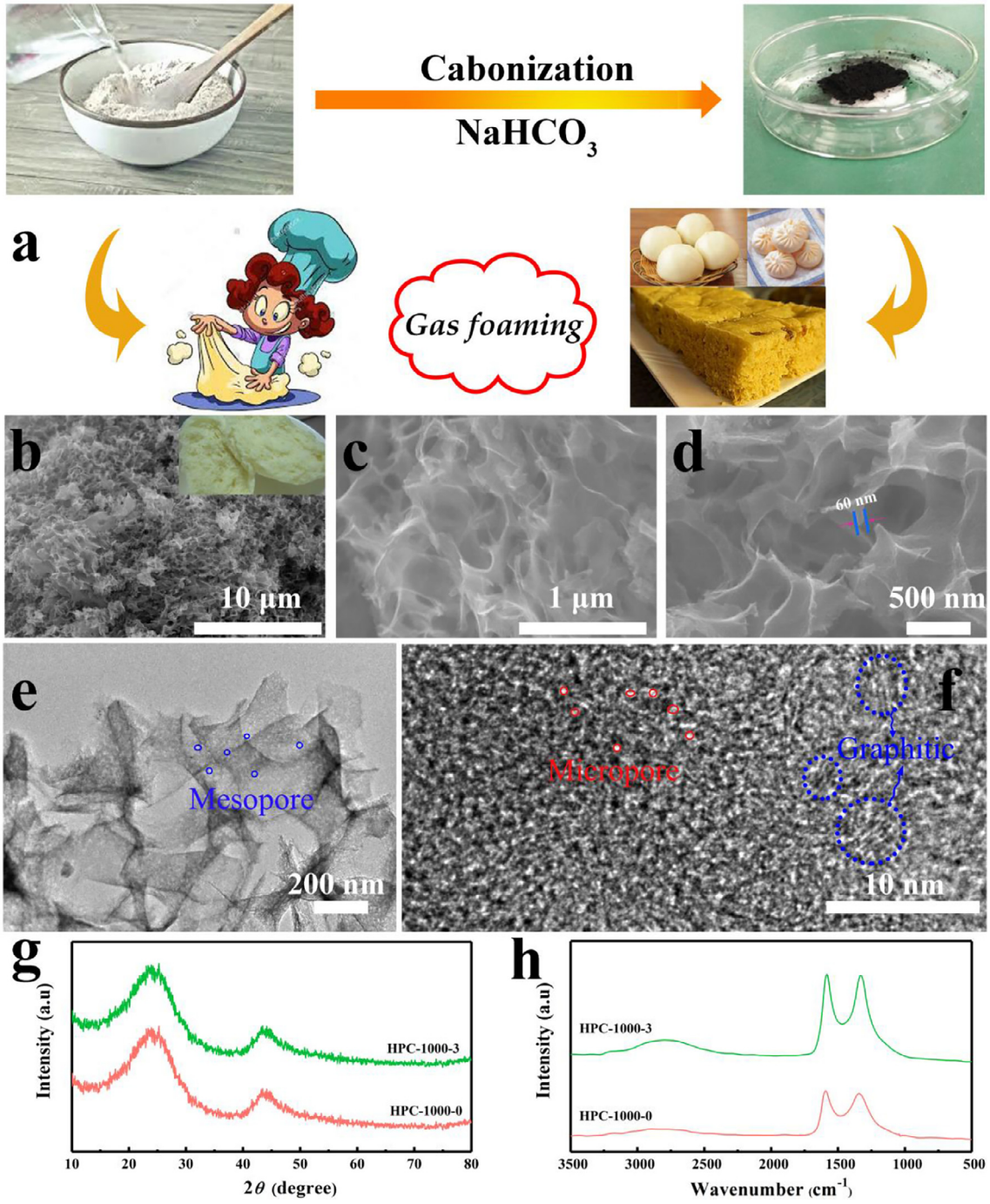

Fig. 1. Schematic illustration of the formation of HPC (a). The SEM images of HPC-1000-3 under different magnifications (b, c and d). The TEM image (e) and HRTEM image (f) of HPC-1000-3. The XRD patterns (g) and Raman spectrogram of HPC-1000-0 and HPC-1000-3.

by the decomposition of $NaHCO_3$.

Based on the above analysis, the as-prepared HPC-1000-3 sample possesses a high specific surface area, well-defined hierarchical pores (containing micro-, meso- and macropores) and certain O-containing surface groups, may ensure the accessibility electro-active surface area and enhance the ion and electron transport rate, which guarantee a good performance for energy storage[38,39]. To evaluate the electrochemical capacitive performance of the as-synthesized carbon materials, CV and GCD, and EIS were first performed in a three-electrode system with an aqueous electrolyte of 6 mol L^{-1} KOH. The CV curves recorded at 100 mV s^{-1} and GCD curves measured at 5 A g^{-1} of the HPC-1000-0, PC-1000 and HPC-1000-3 samples are shown in Fig. 3a and b, respectively. The slightly distorted CV shape and nearly dissymmetry GCD curves indicate the electrochemical capacitor performance is contributed by the combined EDLC performance and the pseudocapacitive behaviour of the O functional groups [40–42]. The pseudo-capacitance reaction of electroactive oxygen species on the carbon surface could be provided in a basic electrolyte as follows [43]:

$$-C-OH + OH^- \leftrightarrow -CO^- + H_2O \quad (1\text{-}9)$$

$$-C{=}O^- + OH^- \leftrightarrow -COOH + e^- \quad (1\text{-}10)$$

$$-COOH + OH^- \leftrightarrow -C{=}O-O^- + H_2O \quad (1\text{-}11)$$

Apparently, compared with the direct carbonized HPC-1000-0 sample, the samples of using $NaHCO_3$ and Na_2CO_3 both exhibited

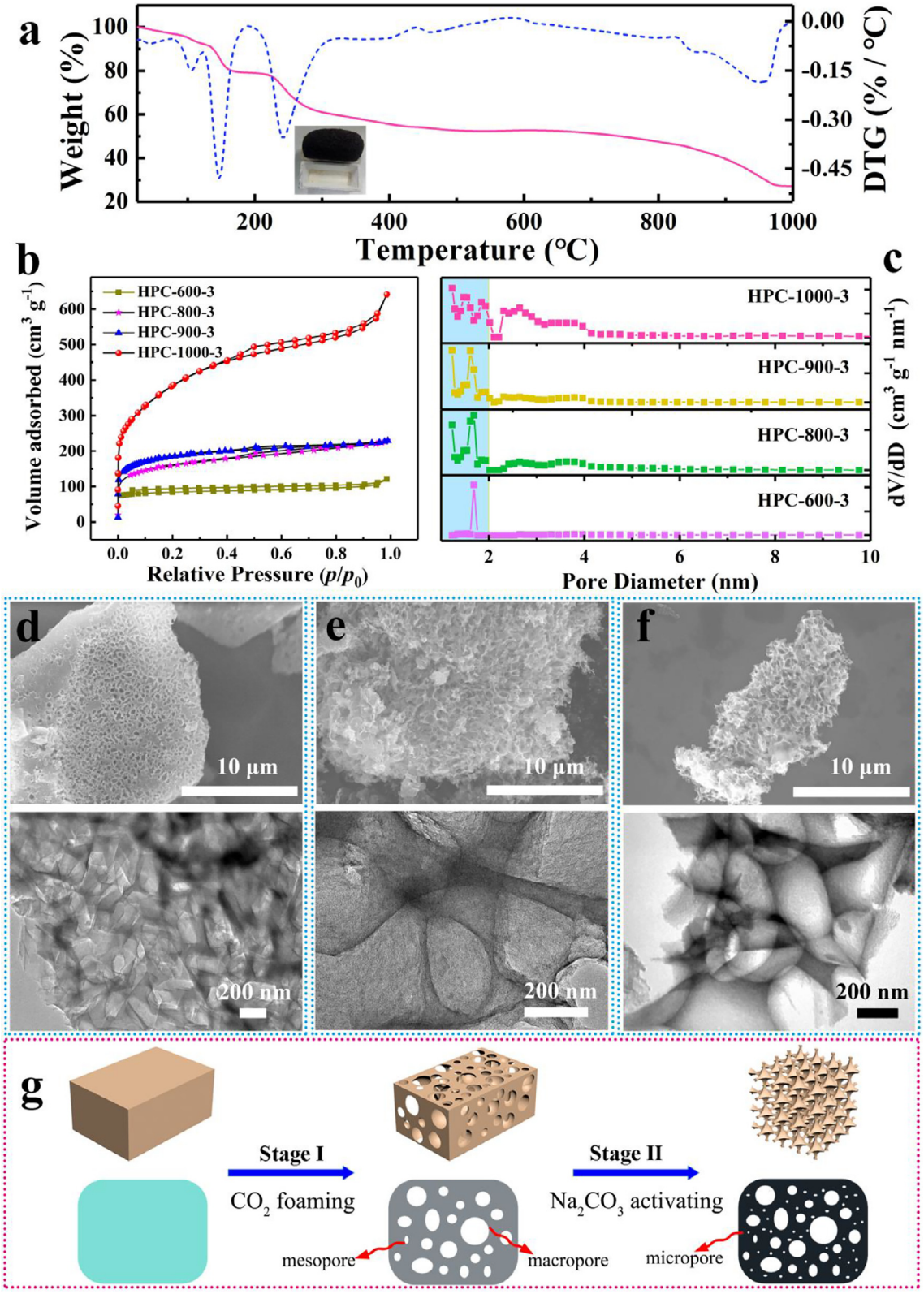

Fig. 2. (a) TG and DTG curves of mixture (the mass weight of flour and $NaHCO_3$ are 6 g and 3 g, respectively), the inset is the digital image of mixture calcined at 250 °C. The N_2 adsorption-desorption isotherms (b) and the corresponding pore size distribution (c) of HPC samples prepared at different temperature. The SEM and TEM images of HPC-600-3 (d), HPC-800-3 (e) and HPC-900-3 (f). Illustration of the growth mechanism of HPC (g).

largely improved electrochemical performance, highlighting the significant role of $NaHCO_3$ and Na_2CO_3 activation. The CV curves of the HPC-1000-3 collected at a scan rate ranging from 10 to 400 mV s^{-1} are depicted in Fig. S6. Clearly, the rectangular CV curve has maintained even at high scan rate of 400 mV s^{-1}, demonstrating a fast kinetics for the formation of an EDLC, a good rate capability and low internal resistance. Furthermore, Fig. S7 provides the dependence of the capacitive current (extracted from the CV curves at −0.5 V) on the applied

Table 1
Pore structural parameters and compositions of HPC-1000-0, HPC-1000-3 and PC-1000, respectively.

	SSA [$m^2\ g^{-1}$]	V_{total}[a] [$cm^3\ g^{-1}$]	V_{mic}[b] [$cm^3\ g^{-1}$]	V_{meso}[c] [$cm^3\ g^{-1}$]	I_D/I_G	Elemental analysis			
						C%	N%	O%	H%
HPC-1000-3	1376	0.99	0.36	0.63	0.987	83.51	0.41	15.51	0.57
HPC-1000-0	456	0.22	0.14	0.08	0.954	87.44	1.68	9.46	1.42
PC-1000	739	0.40	0.25	0.15	0.971	83.78	0.52	14.98	0.72

[a] Specific surface area based on BET equation. [b] The total pore volume was determined from the nitrogen adsorption at pressure of 0.99. [c] Specific surface area of micropores obtained from *t*-plot method.

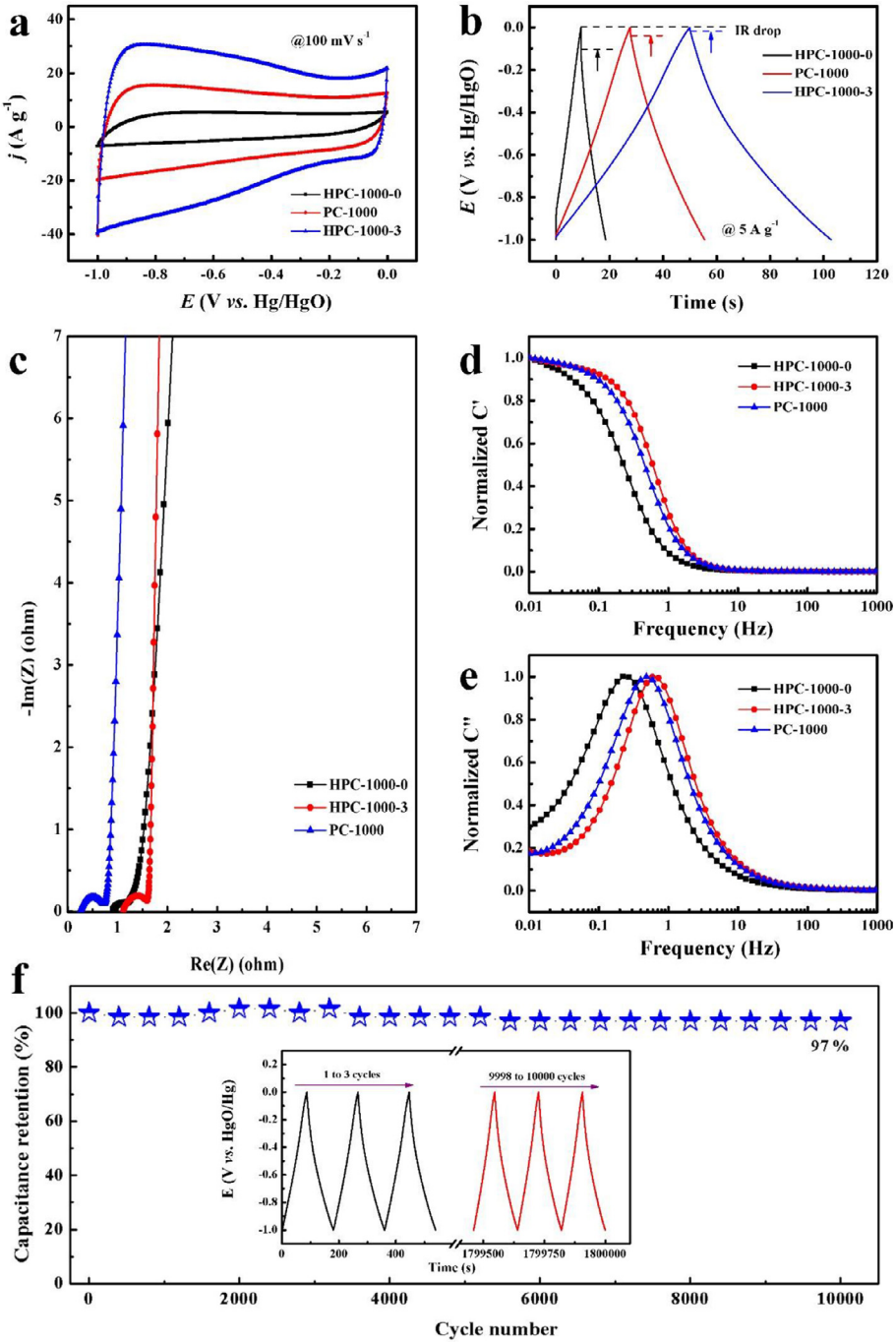

Fig. 3. Comparison of CV curves recorded at 100 mV s^{-1} (a) and GCD curves measured at 3 A g^{-1} (b) of the HPC-1000-0, PC-1000 and HPC-1000-3 samples, respectively. The Nyquist impedance plots (c) and normalized real capacitance (d) and imaginary part capacitance (e) of the HPC-1000-0, PC-1000 and HPC-1000-3 samples, respectively. (f) Cycling stability measured at 5 A g^{-1}, the inset is the GCD curves of the initial three cycles and the last three cycles of 10,000 cycles. The inset: the magnified galvanostatic charge-discharge curves before and after 10,000 cycles.

scan rates of HPC-1000-3. Obviously, a good linear relationship is obtained, which also indicates a remarkably fast charge/discharge capability. Such features nicely supporting our anticipation on the $NaHCO_3$ activation to form an interconnected hierarchical porous structure, which could further facilitate the electrolyte ions transport and diffusion. The GCD curves of the as-prepared samples at various current densities are exhibited in Fig. S6. It is worth emphasizing that the IR drop of HPC-1000-3 is smaller than the HPC-1000-0 and PC-1000, and even at a high discharge current density of 50 A g^{-1}, the IR drop exhibits a quite small value of 0.09 V (Fig. S8), meaning a low internal series resistance. The specific capacitance of HPC-1000-3 is 350 F g^{-1} at low current of 1 A g^{-1} and the specific capacitance can still be maintained to 215.0 F g^{-1} with the current density increases to an ultrahigh value of 50 A g^{-1}, which is higher than that of HPC-1000-0 and PC-1000, and most of reported previously reported porous carbon materials (Table S3), further confirming the high-rate ion and electron transfer of HPC-1000-3. The EIS recorded at a frequency range from 100 kHz to 0.1 Hz was performed to further elucidate the kinetics of ion and electron transport of the as-prepared samples. As shown in Fig. 3c, the spectra contains the steep linear curve in the low frequency region and a semi-circle in the high frequency region, the former represents the charges accumulation electrode/electrolyte interface and the latter indicates the charge transfer resistance. Obviously, the HPC-1000-3 electrode exhibits the steeper straight line (about 86°) than that of the HPC-1000-0 and PC-1000 electrodes, indicating an ideally capacitive behavior, which agrees well with the CV and GCD results. For the high frequency, the diameter of the semicircle is regarded as the equivalent series resistance of the charge-transfer resistance (*R*ct) at the electrode/electrolyte interface. It can be found that HPC-1000-3 has the low equivalent series resistance of 0.50 Ω, reflecting that the electrochemical reaction occur on the HPC-1000-3 electrodes is much easier than other electrodes, which benefited from the interconnect pore framework can effectively reduce ion diffusion path and thus enhance the high electron and ion diffusion rate. More importantly, Bode phase plots of the frequency response of capacitance also reveal the significant influence of the porous structure on the rate of ion transport. The function between cell capacitance $C'(w)$ and the imaginary part $C''(w)$ versus frequency were calculated based on the followed equations, and the results are shown in Fig. 3d and e.

$$C'(w) = \frac{-Z''(w)}{w|Z(w)|^2} \tag{1-12}$$

$$C''(w) = \frac{Z'(w)}{w|Z(w)|^2} \tag{1-13}$$

where Z'' and Z' means the respective real and imaginary parts of the electrochemical impedance Z(w), respectively, and w is the angular frequency which is given by $w = 2\pi f$ (f is the frequency). The HPC-1000-3 has an operating frequency f_0 (f_0, the frequency that the capacitance reaches a 50% of the maximum value) of 0.59 Hz, higher than HPC-1000-0 (0.22 Hz), and PC-1000 (0.48 Hz). When defining a relaxation time constants as $\tau_0 = 1/f_0$, thus the τ_0 of HPC-1000-3, HPC-1000-0 and PC-1000 are 1.69, 2.08 and 4.55 s, respectively. This means that the HPC-1000-3 electrode can deliver its stored energy faster than other electrodes, which is an important role for power capacitor [8]. The long-time cycle stability of electrode materials is another critical requirement for practical applications. Fig. 3f shows the capacitance retention of HPC-1000-3 with cycle number. It is interesting that the capacitance retention increases after slightly decreasing during this cyclic charge-discharge process, which may be due to the effects from doped heteroatoms or in situ activation of the electrode to expose additional surface area [44]. After 10,000 cycles at current density of 3 A g^{-1}, the capacitive retention is still as high as 97% of the initial capacitance, which demonstrate an excellent cycling stability. Besides wheat flour, two other kinds of waste biomasses (rice husk and walnut shell) have been converted to HPC by using $NaHCO_3$ as activator. The precursory waste biomass and their corresponding SEM images and electrochemical performance are shown in Fig. S9. The derived carbon materials also exhibited a 3D porous structure and comparable capacitance performance. It is believed that this chemical foaming stratagem may provide a high-throughput fabrication route for the development of high capacitance carbon materials.

According to the calculating formula $E = CV^2/2$, the working voltage (E) contributes more than that of specific capacitance (C) in depending the energy density of overall supercapacitors [45]. Generally, the working voltage is closely related to the property of the applied electrolyte. The aqueous electrolyte is widely used as electrolyte in supercapacitor in term of its high electrical conductivity, low cost and nonflammable compared with that of organic electrolyte or ionic liquid systems. Unfortunately, the thermodynamic stable potential window of water is only 1.23 V. To increase the working voltage of aqueous electrolyte, the most promising approach is using medium electrolyte (such as Li_2SO_4, Na_2SO_4) and a higher voltage of 1.8–2.0 V can be obtained, which is mainly attributed to low H^+ and OH^- concentration, oxygenated surface functionalities on carbon surface that result in high over-potential for HER and OER under the steady state of the electrode [46,47]. Therefore, to further simulate the actual device behaviour, the electrochemical performance of HPC-1000-3 based supercapacitors was evaluated in a fully assembled two-electrode cell with the 1 mol L^{-1} Na_2SO_4 electrolyte. The electrochemical test of HPC-1000-3 performed on a three-electrode system in 1 mol L^{-1} Na_2SO_4 electrolyte is shown in Fig. S10. Obviously, the HPC-1000-3 electrode has a larger capacitance in KOH electrolyte (350 F g^{-1}) than in Na_2SO_4 (263 F g^{-1}), which is consisting with the pervious results that dictates an alkaline condition is more favorable for redox reactions based on O functional groups. Fig. 4a displays the CV curves of as-fabricated HPC-1000-3 based symmetric supercapacitor operated in different voltage windows at 50 mV s^{-1}. Clearly, when the voltage expanded to 1.8 V, the shape of CV still retain a quasi-rectangular, and also displayed no obvious distortion even at a high scan of 1000 mV s^{-1} (Fig. S11), indicating that the symmetric supercapacitor can be operated at 1.8 V due to the high over-potential for di-hydrogen evolution[48]. Therefore, the potential range is chosen as 1.8 V for the further electrochemical test. Moreover, the rectangular shape of the CV curves at various scanning rates can be kept quite well without a drastic change, suggesting an ideal capacitive behavior and remarkable rate performance probably owing to the unique hierarchical porous nano-structure that favours fast ionic motion. The specific capacitances of symmetric supercapacitor were also calculated based on the GCD curves and the results are provided in Fig. 4c. The calculated specific capacitance was estimated to be 61.6, 51.6, 42.7, 38.8, 36.6 and 33.3 F g^{-1} at current densities of 0.5, 1, 5, 10, 15 and 20 A g^{-1} (based on a symmetric supercapacitor), respectively. The Ragone plot with energy density and power density based on the total weight of electroactive materials in two electrodes are shown in Fig. 4e. It is worth noting that benefitting from its high specific capacitance (61.6 F g^{-1}) and a wide operating voltage (1.8 V), the HPC-1000-3// HPC-1000-3 symmetrical supercapacitor delivers a maximum energy density of 27.4 Wh kg^{-1} at a current density of 0.5 A g^{-1}, to the best of our knowledge, which is the higher than that of previously reported carbon-based symmetric supercapacitors in aqueous electrolytes [27,49–53]. Recently, Compared with gravimetric performance, volumetric performance is a much more reliable parameter for evaluating the capacitance performance due to the limit space in the particle application[54]. We have calculated the volumetric performance in Figs. S12 and S13. The HPC-1000-3 electrode displays a high volumetric capacitance up to 235 F cm^{-3} at 1 A g^{-1}. In addition, HPC-1000-3// HPC-1000-3 symmetrical supercapacitor delivers a maximum energy density of 18.4 Wh L^{-1} at power density of 298.1 W L^{-1}, higher than previously reported carbon-based symmetric supercapacitors in aqueous electrolytes [55–58]. More importantly, the as-assembled HPC-1000-3//HPC-1000-3 supercapacitor shows an excellent cycling stability with 100% capacitance retention after 10,000 cycles at 4 A g^{-1}. The

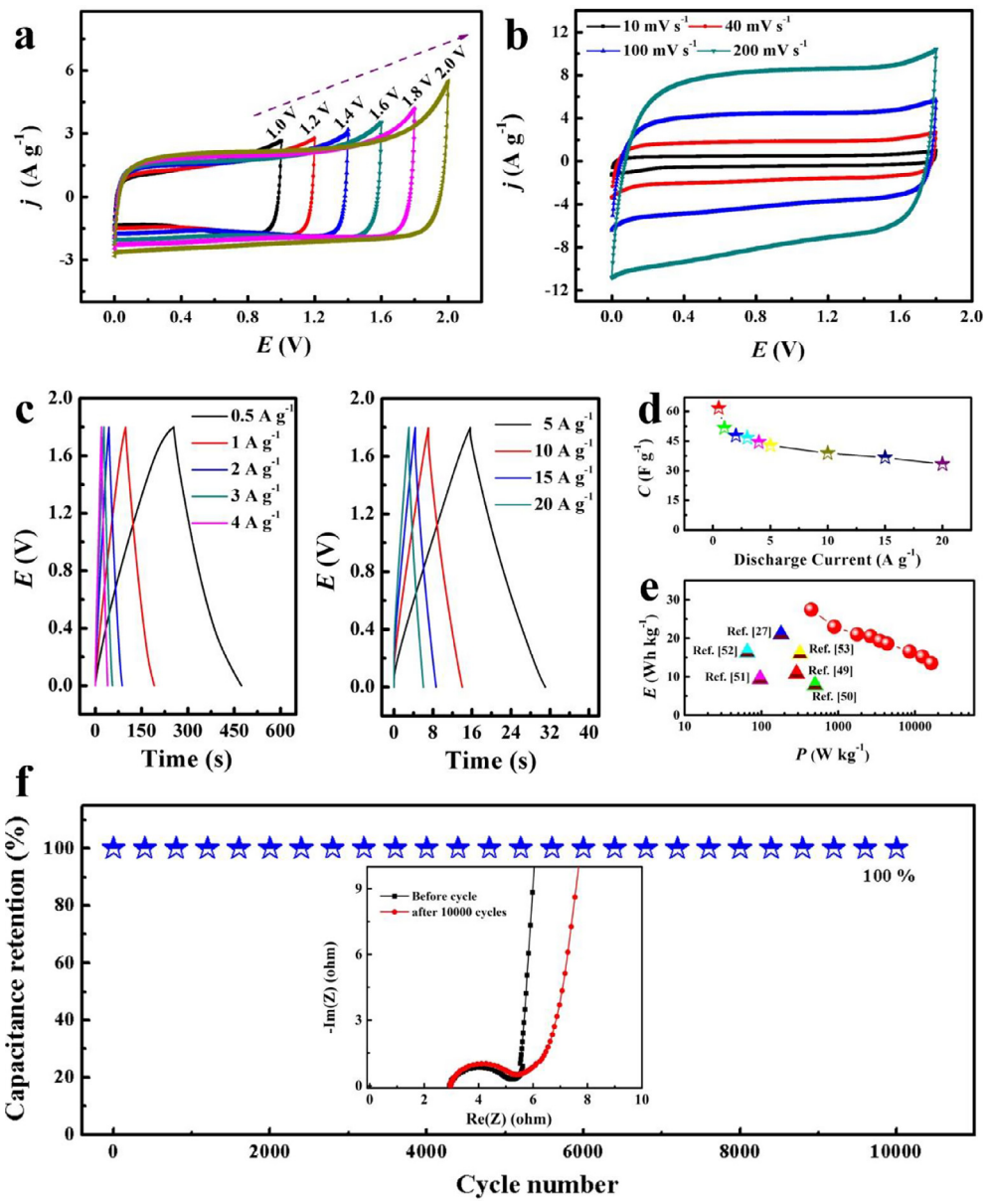

Fig. 4. Electrochemical performance of the HPC-1000-3//HPC-1000-3 symmetrical supercapacitor. (a) CV curves with different operation voltages recorded at the scan rate of 50 mV s^{-1}. (b) CV curves at different scan rates in the voltage window of 0–1.8 V. (c) The GCD curves at different current densities. (d) Specific capacitances based on the total mass of the active materials of the two electrodes at current densities. (e) Ragone plots of the HPC-1000-3//HPC-1000-3 symmetrical supercapacitor and other previously reported carbon based symmetric supercapacitors. (f) Cycling stability at 4 A g^{-1} for 10,000 cycles. The insert is the EIS spectra before and after cycling.

Nyquist plot (the inset of Fig. 4f) shows a linear part at the low-frequency region and a small semicircle at the high frequency region. In the high frequency area, the diameter of the semicircle indicated the charge-transfer impedance (Rct), which is as low as 2.5 Ω for the pristine electrode, and after 10,000 charge-discharge cycles increase to 3.0 Ω, suggesting the HPC-1000-3 electrode have an easier electrolyte ion access and better charge transfer.

The superior electrochemical performances of the HPC-1000-3 sample may be attributed to the followed reasons: (1) The high specific surface area of the as-prepared HPC sample could provide sufficient active sites for ion adsorption to accommodate a large amount of charges; (2) The hierarchically interconnected pores structure could effectively reduce the pathway of ion diffusion and the partial graphitization area could severs as a highway for electron transportation, which will resulting in an enhanced charge storage and high rate; (3) The O functional groups can not only contribute pseudocapacitance to the overall capacitance and also enhance the wettability of the electrode, facilitate the ion fast transportation.

6. Conclusions

In summary, a honeycomb-like porous carbon material has been synthesized via fermentation approach using flour as the basic element. Due to the large surface area (1376 $m^2 g^{-1}$), excellent interconnectivity and heteroatom doping, the as-obtained samples exhibit high specific capacitance of 350 F g^{-1} at 1 A g^{-1} and outstanding electrochemical stability with capacitance retention up to 97% after 10,000 cycles. Moreover, the as-assembled symmetric supercapacitor delivers high energy densities of 27.4 Wh kg^{-1}, as well as excellent cycling performance. It is believed that this study may provide a new route for the development of novel HPC-based electrode materials. In addition, it also shows attractive prospects for potential industrial application in energy storage, adsorbents, catalysts, gas storage.

Acknowledgment

We gratefully acknowledge the financial support of this research by National Nature Science Foundation of China (21503055), the Hong Kong Scholars Programs (Grant No. XJ2016046), the China Postdoctoral Science Foundation (2015M571390), the Natural Science

Foundation of Heilongjiang Province of China (QC2015015), the Heilongjiang Postdoctoral Fund (LBHZ14054, LBH-TZ0609) and Fundamental Research Funds for the Central Universities (HEUCF181007).

Appendix A. Supplementary data

Supplementary data associated with this article can be found, in the online version, at https://doi.org/10.1016/j.cej.2018.06.184.

References

[1] M. Sevilla, R. Mokaya, Energy storage applications of activated carbons: supercapacitors and hydrogen storage, Energy Environ. Sci. 7 (2014) 1250–1280.
[2] C. Chen, D. Yu, G. Zhao, B. Du, W. Tang, L. Sun, Y. Sun, F. Besenbacher, M. Yu, Three-dimensional scaffolding framework of porous carbon nanosheets derived from plant wastes for high-performance supercapacitors, Nano Energy 27 (2016) 377–389.
[3] G. Qu, J. Cheng, X. Li, D. Yuan, P. Chen, X. Chen, B. Wang, H. Peng, A fiber supercapacitor with high energy density based on hollow graphene/conducting polymer fiber electrode, Adv. Mater. 28 (2016) 3646–3652.
[4] L.L. Zhang, X.S. Zhao, Carbon-based materials as supercapacitor electrodes, Chem. Soc. Rev. 38 (2009) 2520–2531.
[5] Z.-Y. Yu, L.-F. Chen, L.-T. Song, Y.-W. Zhu, H.-X. Ji, S.-H. Yu, Free-standing boron and oxygen Co-doped carbon nanofiber films for large volumetric capacitance and high rate capability supercapacitors, Nano Energy 15 (2015) 235–243.
[6] P. Simon, Y. Gogotsi, Materials for electrochemical capacitors, Nat. Mater. 7 (2008) 845–854.
[7] K.-L. Hong, L. Qie, R. Zeng, Z.-Q. Yi, W. Zhang, D. Wang, W. Yin, C. Wu, Q.-J. Fan, W.-X. Zhang, Y.-H. Huang, Biomass derived hard carbon used as a high performance anode material for sodium ion batteries, J. Mater. Chem. A 2 (2014) 12733–12738.
[8] M.D. Stoller, R.S. Ruoff, Best practice methods for determining an electrode material's performance for ultracapacitors, Energy Environ. Sci. 3 (2010) 1294–1301.
[9] X. Wei, X. Jiang, J. Wei, S. Gao, Functional groups and pore size distribution do matter to hierarchically porous carbons as high-rate performance supercapacitors, J. Mater. Chem. 28 (2016) 445–458.
[10] L. Wei, G. Yushin, Nanostructured activated carbons from natural precursors for electrical double layer capacitors, Nano Energy 1 (2012) 552–565.
[11] X. Wei, S. Wan, S. Gao, Self-assembly-template engineering nitrogen-doped carbon aerogels for high-rate supercapacitors, Nano Energy 28 (2016) 206–215.
[12] R. Ryoo, S.H. Joo, S. Jun, Synthesis of highly ordered carbon molecular sieves via template-mediated structural transformation, J. Phys. Chem. B 103 (1999) 7743–7746.
[13] J. Wei, D. Zhou, Z. Sun, Y. Deng, Y. Xia, D. Zhao, A controllable synthesis of rich nitrogen-doped ordered mesoporous carbon for CO_2 capture and supercapacitors, Adv. Funct. Mater. 23 (2013) 2322–2328.
[14] H. Nishihara, T. Kyotani, Templated nanocarbons for energy storage, Adv. Mater. 24 (2012) 4473–4498.
[15] B. Hu, K. Wang, L. Wu, S.-H. Yu, M. Antonietti, M.-M. Titirici, Engineering carbon materials from the hydrothermal carbonization process of biomass, Adv. Mater. 22 (2010) 813–828.
[16] H. Teng, S.-C. Wang, Influence of oxidation on the preparation of porous carbons from phenol – formaldehyde resins with KOH activation, Ind. Eng. Chem. Res. 39 (2000) 673–678.
[17] Y. Gao, Y.S. Zhou, M. Qian, X.N. He, J. Redepenning, P. Goodman, H.M. Li, L. Jiang, Y.F. Lu, Chemical activation of carbon nano-onions for high-rate supercapacitor electrodes, Carbon 51 (2013) 52–58.
[18] L. Qie, W. Chen, H. Xu, X. Xiong, Y. Jiang, F. Zou, X. Hu, Y. Xin, Z. Zhang, Y. Huang, Synthesis of functionalized 3D hierarchical porous carbon for high-performance supercapacitors, Energy Environ. Sci. 6 (2013) 2497–2504.
[19] B. Jache, C. Neumann, J. Becker, B.M. Smarsly, P. Adelhelm, Towards commercial products by nanocasting: characterization and lithium insertion properties of carbons with a macroporous, interconnected pore structure, J. Mater. Chem. 22 (2012) 10787–10794.
[20] M.J. Bleda-Martínez, J.A. Maciá-Agulló, D. Lozano-Castelló, E. Morallón, D. Cazorla-Amorós, A. Linares-Solano, Role of surface chemistry on electric double layer capacitance of carbon materials, Carbon 43 (2005) 2677–2684.
[21] D. Zhai, B. Li, H. Du, G. Wang, F. Kang, The effect of pre-carbonization of mesophase pitch-based activated carbons on their electrochemical performance for electric double layer capacitors, J. Solid. State. Electr. 15 (2011) 787–794.
[22] D. Lozano-Castelló, D. Cazorla-Amorós, A. Linares-Solano, S. Shiraishi, H. Kurihara, A. Oya, Influence of pore structure and surface chemistry on electric double layer capacitance in non-aqueous electrolyte, Carbon 41 (2003) 1765–1775.
[23] T. Ouyang, K. Cheng, Y. Gao, S. Kong, K. Ye, G. Wang, D. Cao, Molten salt synthesis of nitrogen doped porous carbon: a new preparation methodology for high-volumetric capacitance electrode materials, J. Mater. Chem. A 4 (2016) 9832–9843.
[24] L. Xie, G. Sun, F. Su, X. Guo, Q. Kong, X. Li, X. Huang, L. Wan, W. Song, K. Li, C. Lv, C.-M. Chen, Hierarchical porous carbon microtubes derived from willow catkins for supercapacitor applications, J. Mater. Chem. A 4 (2016) 1637–1646.
[25] Y. Yuan, Y. Ding, C. Wang, F. Xu, Z. Lin, Y. Qin, Y. Li, M. Yang, X. He, Q. Peng, Y. Li, Multifunctional stiff carbon foam derived from bread, ACS. Appl. Mater. Inter. 8 (2016) 16852–16861.
[26] L.-F. Chen, Z.-H. Huang, H.-W. Liang, Q.-F. Guan, S.-H. Yu, Bacterial-cellulose derived carbon nanofiber@MnO_2 and nitrogen-doped carbon nanofiber electrode materials: an asymmetric supercapacitor with high energy and power density, Adv. Mater. 25 (2013) 4746–4752.
[27] Y. Li, G. Wang, T. Wei, Z. Fan, P. Yan, Nitrogen and sulfur Co-doped porous carbon nanosheets derived from willow catkin for supercapacitors, Nano Energy 19 (2016) 165–175.
[28] X. Wu, L. Jiang, C. Long, Z. Fan, From flour to honeycomb-like carbon foam: carbon makes room for high energy density supercapacitors, Nano Energy 13 (2015) 527–536.
[29] S. Gao, X. Li, L. Li, X. Wei, A versatile biomass derived carbon material for oxygen reduction reaction, supercapacitors and oil/water separation, Nano Energy 33 (2017) 334–342.
[30] S. Gao, Y. Chen, H. Fan, X. Wei, C. Hu, H. Luo, L. Qu, Large scale production of biomass-derived N-doped porous carbon spheres for oxygen reduction and supercapacitors, J. Mater. Chem. A 2 (2014) 3317–3324.
[31] X. Zhao, Q. Zhang, C.-M. Chen, B. Zhang, S. Reiche, A. Wang, T. Zhang, R. Schlögl, D. Sheng Su, Aromatic sulfide, sulfoxide, and sulfone mediated mesoporous carbon monolith for use in supercapacitor, Nano Energy 1 (2012) 624–630.
[32] W. Shen, W. Fan, Nitrogen-containing porous carbons: synthesis and application, J. Mater. Chem. A 1 (2013) 999–1013.
[33] M. Zhou, F. Pu, Z. Wang, S. Guan, Nitrogen-doped porous carbons through KOH activation with superior performance in supercapacitors, Carbon 68 (2014) 185–194.
[34] Y. Zhao, S. Huang, M. Xia, S. Rehman, S. Mu, Z. Kou, Z. Zhang, Z. Chen, F. Gao, Y. Hou, N-P-O co-doped high performance 3D graphene prepared through red phosphorous-assisted "cutting-thin" technique: a universal synthesis and multifunctional applications, Nano Energy 28 (2016) 346–355.
[35] Y. Zhao, W. Ran, J. He, Y. Song, C. Zhang, D.-B. Xiong, F. Gao, J. Wu, Y. Xia, Oxygen-rich hierarchical porous carbon derived from artemia cyst shells with superior electrochemical performance, ACS. Appl. Mater. Inter. 7 (2015) 1132–1139.
[36] T. Ouyang, K. Cheng, F. Yang, J. Jiang, J. Yan, K. Zhu, K. Ye, G. Wang, L. Zhou, D. Cao, A general in-situ etching and synchronous heteroatom doping strategy to boost the capacitive performance of commercial carbon fiber cloth, Chem. Eng. J. 335 (2018) 638–646.
[37] X. Li, C. Tang, M. Ai, L. Dong, Z. Xu, Controllable synthesis of pure phase rare-earth orthoferrites hollow spheres with a porous shell and their catalytic performance for The CO + NO reaction, J. Mater. Chem. 22 (2010) 4879–4889.
[38] D. Carriazo, M.C. Gutiérrez, F. Picó, J.M. Rojo, J.L.G. Fierro, M.L. Ferrer, F. del Monte, Phosphate functionalized carbon monoliths from deep eutectic solvents and their use as monolithic electrodes in supercapacitors, ChemSusChem 5 (2012) 1405–1409.
[39] M.C. Gutiérrez, D. Carriazo, A. Tamayo, R. Jiménez, F. Picó, J.M. Rojo, M.L. Ferrer, F. del Monte, Deep-eutectic-solvent-assisted synthesis of hierarchical carbon electrodes exhibiting capacitance retention at high current densities, Chem.-Eur. J. 17 (2011) 10533–10537.
[40] Y. Yan, T. Kuila, N.H. Kim, J.H. Lee, Effects of acid vapour mediated oxidization on the electrochemical performance of thermally exfoliated graphene, Carbon 74 (2014) 195–206.
[41] Z. Kou, B. Guo, Y. Zhao, S. Huang, T. Meng, J. Zhang, W. Li, I.S. Amiinu, Z. Pu, M. Wang, M. Jiang, X. Liu, Y. Tang, S. Mu, Molybdenum carbide-derived chlorine-doped ordered mesoporous carbon with few-layered graphene walls for energy storage applications, ACS Appl. Mater. Inter. 9 (2017) 3702–3712.
[42] Y. Zhao, Z. Zhang, Y. Ren, W. Ran, X. Chen, J. Wu, F. Gao, Vapor deposition polymerization of aniline on 3D hierarchical porous carbon with enhanced cycling stability as supercapacitor electrode, J. Power Sources 286 (2015) 1–9.
[43] J. Lili, S. Lizhi, L. Conglai, W. Tong, F. Zhuangjun, Functional pillared graphene frameworks for ultrahigh volumetric performance supercapacitors, Adv. Energy Mater. 5 (2015) 1500771.
[44] H. Sun, L. Cao, L. Lu, Bacteria promoted herarchical carbon materials for high-performance supercapacitor, Energy Environ. Sci. 5 (2012) 6206–6213.
[45] Y. Minghao, L. Yongzhuang, Z. Haibing, L. Xihong, New Insights into the Operating Voltage of Aqueous Supercapacitors, Chem.-Eur. J. 24 (2018) 3639–3649.
[46] Q. Gao, L. Demarconnay, E. Raymundo-Pinero, F. Beguin, Exploring the large voltage range of carbon/carbon supercapacitors in aqueous lithium sulfate electrolyte, Energy Environ. Sci. 5 (2012) 9611–9617.
[47] X. Zhang, J. Jiang, Y. Chen, K. Cheng, F. Yang, J. Yan, K. Zhu, K. Ye, G. Wang, L. Zhou, D. Cao, A flexible and high voltage symmetric supercapacitor based on hybrid configuration of cobalt hexacyanoferrate/reduced graphene oxide hydrogels, Chem. Eng. J. 335 (2018) 321–329.
[48] M.P. Bichat, E. Raymundo-Piñero, F. Béguin, High voltage supercapacitor built with seaweed carbons in neutral aqueous electrolyte, Carbon 48 (2010) 4351–4361.
[49] G. Zhang, L. Wang, Y. Hao, X. Jin, Y. Xu, Y. Kuang, L. Dai, X. Sun, Unconventional carbon: alkaline dehalogenation of polymers yields N-doped carbon electrode for high-performance capacitive energy storage, Adv. Funct. Mater. 26 (2016) 3340–3348.
[50] Y. Fan, P. Liu, B. Zhu, S. Chen, K. Yao, R. Han, Microporous carbon derived from acacia gum with tuned porosity for high-performance electrochemical capacitors, Int. J. Hydrogen Energ. 40 (2015) 6188–6196.
[51] Q. Liang, L. Ye, Z.-H. Huang, Q. Xu, Y. Bai, F. Kang, Q.-H. Yang, A honeycomb-like porous carbon derived from pomelo peel for use in high-performance supercapacitors, Nanoscale 6 (2014) 13831–13837.
[52] Q. Wang, J. Yan, Z. Fan, Nitrogen-doped sandwich-like porous carbon nanosheets for high volumetric performance supercapacitors, Electrochim. Acta 146 (2014) 548–555.
[53] Q. Wang, J. Yan, Y. Wang, T. Wei, M. Zhang, X. Jing, Z. Fan, Three-dimensional

flower-like and hierarchical porous carbon materials as high-rate performance electrodes for supercapacitors, Carbon 67 (2014) 119–127.
[54] Q. Wang, J. Yan, Z. Fan, Carbon materials for high volumetric performance supercapacitors: design, progress, challenges and opportunities, Energy Environ. Sci. 9 (2016) 729–762.
[55] E. Raymundo-Piñero, F. Leroux, F. Béguin, A high-performance carbon for supercapacitors obtained by carbonization of a seaweed biopolymer, Adv. Mater. 18 (2006) 1877–1882.
[56] Y. Tao, X. Xie, W. Lv, D.-M. Tang, D. Kong, Z. Huang, H. Nishihara, T. Ishii, B. Li, D. Golberg, F. Kang, T. Kyotani, Q.-H. Yang, Towards ultrahigh volumetric capacitance: graphene derived highly dense but porous carbons for supercapacitors, Sci. Rep. 3 (2013) 2975.
[57] J. Hu, H. Wang, Q. Gao, H. Guo, Porous carbons prepared by using metal–organic framework as the precursor for supercapacitors, Carbon 48 (2010) 3599–3606.
[58] Y. Yoon, K. Lee, S. Kwon, S. Seo, H. Yoo, S. Kim, Y. Shin, Y. Park, D. Kim, J.-Y. Choi, H. Lee, Vertical alignments of graphene sheets spatially and densely piled for fast Ion diffusion in compact supercapacitors, ACS Nano 8 (2014) 4580–4590.